

Optical Engineering

OpticalEngineering.SPIEDigitalLibrary.org

Study of the factors that affect the correlation behavior during the evaluation of interferograms

Brenda Villalobos-Mendoza
Daniel Aguirre-Aguirre
Fermín Granados-Agustín

SPIE.

Brenda Villalobos-Mendoza, Daniel Aguirre-Aguirre, Fermín Granados-Agustín, "Study of the factors that affect the correlation behavior during the evaluation of interferograms," *Opt. Eng.* **57**(10), 104111 (2018), doi: 10.1117/1.OE.57.10.104111.

Study of the factors that affect the correlation behavior during the evaluation of interferograms

Brenda Villalobos-Mendoza,^{a,b,*} Daniel Aguirre-Aguirre,^{a,c} and Fermín Granados-Agustín^d

^aUniversidad Nacional Autónoma de México, Polo Universitario de Tecnología Avanzada, Apodaca, Mexico

^bCentro de Investigación y de Estudios Avanzados del Instituto Politécnico Nacional, Unidad Monterrey, Apodaca, Mexico

^cUniversidad Nacional Autónoma de México, Instituto de Ciencias Aplicadas y Tecnología, Mexico City, Mexico

^dInstituto Nacional de Astrofísica Óptica y Electrónica, San Andrés Cholula, Mexico

Abstract. In recent years, the correlation coefficient has been used as a tool for comparison between experimental and synthetic interferograms in algorithms of evaluation, in the areas of optical fabrication and testing. This coefficient has been used with the aim of eliminating the observer criterion during the fabrication process, and in this sense, to make a quantitative test to compare experimental and synthetic interferograms using the correlation as a parameter of evaluation. However, this coefficient is dramatically affected when laboratory conditions are not adequate. Therefore, in this work, we present a detailed analysis of the correlation behavior when interferograms with different values of visibility, Gaussian noise, and background illumination are evaluated/correlated. To analyze the correlation behavior, we simulated different interferograms, where these parameters were varied and examined how they affect the interference patterns. We found that a bad illumination dramatically affects the value of correlation, causing it to decrease to 0.1046, with $\sigma = 0.1$. © The Authors. Published by SPIE under a Creative Commons Attribution 3.0 Unported License. Distribution or reproduction of this work in whole or in part requires full attribution of the original publication, including its DOI. [DOI: [10.1117/1.OE.57.10.104111](https://doi.org/10.1117/1.OE.57.10.104111)]

keywords: correlation; interferogram evaluation; Ronchi test; optical metrology.

Paper 180941 received Jun. 29, 2018; accepted for publication Sep. 28, 2018; published online Oct. 25, 2018.

1 Introduction

During the fabrication of an optical surface, it is important to know the shape that is being obtained during the fabrication; this is done with the aim of knowing how similar the surface under fabrication (real) is compared with the surface that is intended to be generated (ideal).¹⁻³

To perform metrology on an optical surface, it is necessary to obtain reliable and accurate measurements, as well as a good method of analysis. Within this category, the most common methods used for this purpose are interferometric tests, such as the Fizeau, Newton, Twyman–Green, and Ronchi tests, among others.⁴⁻⁷ In these tests, the interferogram is captured and analyzed to obtain quantitative information about the surface under test.

Given the diversity of images (interferograms), recording devices (CCDs, CMOS), and illumination sources (LEDs, LASER), there exist criteria that determine their analysis and processing.⁸⁻¹⁰ One of these criteria is the need for global uniformity, which implies the same values of brightness; as a consequence, the illumination must be uniform for all images obtained at different times. In the case of an experimental interferogram, capturing an image with good illumination, good visibility, and null Gaussian noise is quite complicated. It is for these reasons that it is of interest to analyze the effect of having different values of visibility, background illumination, and Gaussian noise when an interferogram is evaluated with the correlation criterion.^{11,12}

In optical testing, there are many ways to obtain information from an interferogram, and the wavefront deformations may be easily estimated from a visual estimation of fringe deviation from straightness.¹³ This visual method gives us

a precision that greatly depends on the skills of the person making the measurements.

The simplest quantitative method of analysis involves visually identifying and then tracking the fringes on the interferogram. An image of the interferogram can be taken and then digitalized into a computer to enter the x, y coordinates of some selected points of the interferogram located on the fringes. The objective is to locate the fringe maxima or minima by searching with algorithms based on line tracking, threshold comparison, or adaptive binarization.¹⁴⁻¹⁸ When the maxima have been located, a subsequent fringe thinning or skeletonization is performed. Skeletonizing is based on a search of local irradiance peaks by segmentation algorithms based on adaptive thresholds, gradient operators, and spatial frequency filtering, among others. The result is a skeleton of the interferogram formed by lines one pixel wide.¹⁹

Currently, there are techniques that use all the information captured on the image, so the information is extracted from each pixel. One of these techniques is the phase shifting interferometry,^{10,20} where three or more interference patterns are needed to obtain the wavefront phase. The shift must be known and controlled; otherwise, the recovered information will be erroneous. Other used techniques include the Fourier method²¹ and the synchronous method.²² However, the disadvantage of these techniques is that they do not work when there are closed fringes, or the image has a lot of noise.

Recently, the analyses of interferograms using techniques, such as genetic algorithms,^{23,24} evolutive strategy,^{25,26} and probabilistic estimation,¹⁹ have been investigated. These techniques use methods to compare images that are generated synthetically with images obtained experimentally, to estimate, with a high precision, the value of the phase.

One of the disadvantages of using some of these methods of comparison is that for the synthetic interferogram, the background illumination is uniform, the visibility is always

*Address all correspondence to: Brenda Villalobos-Mendoza, E-mail: bvillalobosmendoza@gmail.com

one, and the Gaussian noise is null, but this is not the case for an experimental interferogram, where these values are different in every captured image. As a result, it is almost impossible to reach a value of 1 in the correlation coefficient when an experimental image is being analyzed. For these reasons, in this work, we decided to analyze the correlation behavior and the maximum value of correlation that can be achieved when these parameters are varied.

This work is organized as follows: in Sec. 2, the mathematical basis of interferometry and some examples of interferograms affected by visibility, Gaussian noise, and inhomogeneous background illumination are shown. Section 3 presents the equation of correlation. In Sec. 4, the correlation behavior is analyzed when the interference patterns are degraded by visibility, Gaussian noise, and inhomogeneous background illumination, as well as their combinations. Section 5 shows some experimental results using two aspherical surfaces. Finally, in Sec. 6, some conclusions are given.

2 Synthetic Interferogram Equations

In physical optics, the interference effect consists of superposing two or more optical fields in a region of space.^{27,28} When this sum is observed with an optical detector, the irradiance of the total field is obtained and can be understood as the sum of the irradiance from each individual field, known as background illumination, plus an additional interference term per each pair of fields, which consists of the cosine of the phase difference between the two waves and a factor

given primarily by the product of wave amplitudes, known as a modulation light.²⁷ The total effect shows bright and dark zones known as interference fringes, also called a fringe pattern or interferogram. The irradiance function in the interference patterns may be written as follows:

$$I(x, y) = a(x, y) + b(x, y) \cos \phi, \tag{1}$$

where $a(x, y) = I_1(x, y) + I_2(x, y)$ and $b(x, y) = 2[I_1(x, y)I_2(x, y)]^{1/2}$ correspond to the background illumination and local contrast, respectively; the phase is given by ϕ .

2.1 Visibility

Because common sources have finite extension, we must examine how such extension affects the fringes. Assuming that the variation of $a(x, y)$ and $b(x, y)$ inside the interferogram aperture is smoother than the variations of the cosine term in Eq. (1), the maximum irradiance in the vicinity of the point in the interferogram is given by

$$I_{\max}(x, y) = I_1(x, y) + I_2(x, y) + 2\sqrt{I_1(x, y)I_2(x, y)}. \tag{2}$$

The minimum irradiance in the same vicinity is given by

$$I_{\min}(x, y) = I_1(x, y) + I_2(x, y) - 2\sqrt{I_1(x, y)I_2(x, y)}, \tag{3}$$

and the fringe visibility $\nu(x, y)$, is defined by

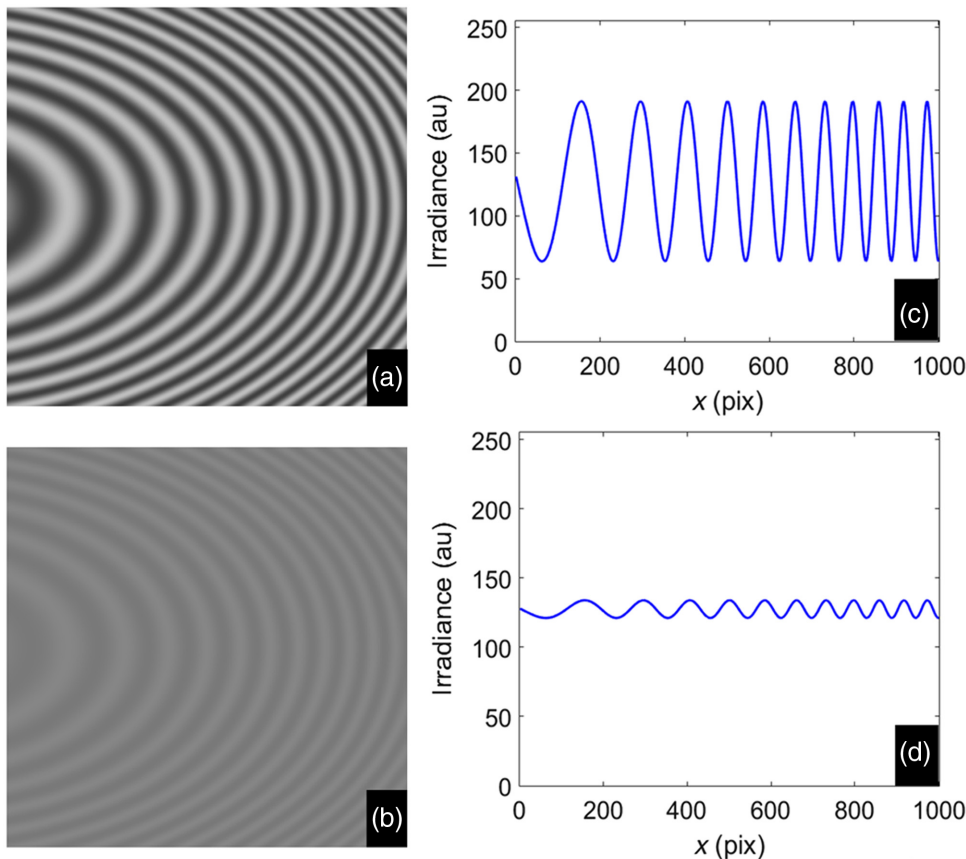


Fig. 1 Interferograms with visibilities of (a) 0.5 and (b) 0.05, and central profile of images with visibilities of (c) 0.5 and (d) 0.05.

$$v(x, y) = \frac{I_{\max}(x, y) - I_{\min}(x, y)}{I_{\max}(x, y) + I_{\min}(x, y)}, \quad (4)$$

where I_{\max} and I_{\min} are the maximum and minimum irradiances, respectively.^{8,27} Clearly, $v(x, y)$ has a maximum value of unity when $I_{\min} = 0$, as is the case for fringes from two equal monochromatic point sources, and decreases to zero when $I_{\max} = I_{\min}$, and the fringes disappear. In Fig. 1, some examples of interferograms generated with different visibilities are shown.

As can be seen in Figs. 1(a) and 1(b), as the value of visibility moves away from 1, the contrast in the interferogram decreases until the fringes almost disappear. In Figs. 1(c) and 1(d), the central profiles of the interferograms are shown, where the amplitude of the intensity decreases as the visibility does. Note in Fig. 1 that as the value of the visibility increases, the contrast obtained in each plot also increases.

2.2 Gaussian Noise

Electronic noise in photodetectors is recognized as a random fluctuation of the measured voltage or current and is caused by the quantum nature of matter.²⁹ The first category of noise sources is due to the photodetector as an electronic component: noise is generated even without impinging light. Thermal noise, generation-recombination noise, and the $1/f$ noise fall into this category.²⁹⁻³¹ The second category contains the additional noise generated when photons impinge on the detector, known as photon or shot noise.

Electronic noise is the sum of numerous random process obeying different statistical laws, but the central limit theorem of probability theory states that the overall process will be directed by a Gaussian distribution.²⁹

In this work, the noise introduced in every interferogram shows a density of probability that obeys a normal distribution commonly called a Gaussian distribution. For the generation of this kind of noise, a function of MATLAB™ called “rand” was used. This function generates Gaussian values with a median of zero and a variance of one.³² For values with mean and variance different to that used, it must multiply the value of each pixel image by the desired standard deviation (η) and to add the mean (μ) in the next form:

$$X = \eta \text{randn} + \mu. \quad (5)$$

For measuring the noise introduced to the synthetic interferograms, the peak signal-to-noise ratio (PSNR), which is a relative measure of the quality of the image, was used.³³ This measure is based on the mean square error (MSE) given by the next expression:

$$\text{MSE} = \frac{1}{mn} \sum_{x=1}^n \sum_{y=1}^m [R(x, y) - R'(x, y)]^2, \quad (6)$$

where m and n represent the number of rows and columns of the image, respectively; $R(x, y)$ corresponds to the original image, and $R'(x, y)$ is the image with noise.

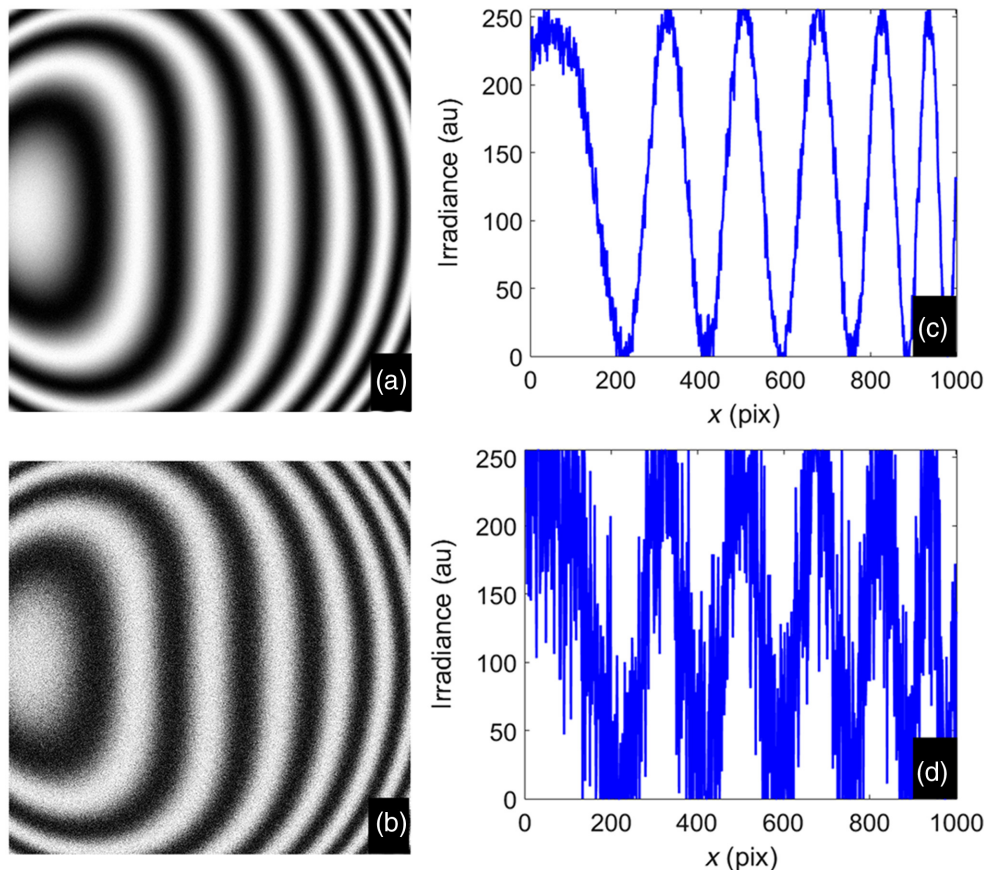


Fig. 2 Varying the Gaussian noise. (a) $\eta = 10$, $\mu = 0$; PSNR = 28.6776 dB and (b) $\eta = 70$, $\mu = 0$; PSNR = 13.1155 dB, and central profiles of (c) 28.6776 dB and (d) 13.1155 dB.

Using the MSE, we can obtain the PSNR, defined as follows:

$$\text{PSNR} = 10 \log_{10} \frac{|Pi|^2}{\text{MSE}}, \tag{7}$$

where Pi is the maximum signal value that exists in our original image, commonly not needed because it is not common to have a negative value of the pixel. For binary images, the numerator will be always one. For images with gray scale and with 8 bits by pixel, the numerator is 255. For color images only, the luminance component is used.³³

A great similarity between the images implies a low value of MSE, and it results in a high value of PSNR. A high value of PSNR is good because it means that the image has low noise. The PSNR is a dimensionless number because the units of the numerator and denominator are the same. However, because of the use of the logarithmic scale, the PSNR is expressed in decibels (dB); experimental images captured in the laboratory commonly have values between 20 and 40 dB.^{33,34} In Fig. 2, some interference patterns are shown with different levels of noise. As can be seen in Fig. 2, the image starts to degrade as the level of noise increases.

2.3 Inhomogeneous Background Illumination

There are many reasons for an uneven background illumination in the interference patterns; one reason may be that the

beam profile of the illuminating source is modified by the projecting optics, in most cases, a Gaussian intensity profile. Another reason can be an uneven reflectivity of the object surface caused by a spatially varying surface characteristic, among many others.

In our case, to simulate synthetic interferograms with inhomogeneous background illumination, we added to Eq. (1), a Gaussian function given by

$$G(x, y) = A \exp \left[-\frac{(x - \Delta x)^2 + (y - \Delta y)^2}{2\sigma^2} \right], \tag{8}$$

where A represents the amplitude of the Gaussian function, Δx and Δy are displacements of the center of the Gaussian in the x and y axes, respectively, and σ represents the Gaussian width.

The inhomogeneous background illumination is added to each image in the next form:

$$I_{\text{new}}(x, y) = \frac{I(x, y) * G(x, y)}{Pi}. \tag{9}$$

In Fig. 3, some interference patterns are shown with inhomogeneous background illumination, varying σ and maintaining Δx and $\Delta y = 0$.

As can be seen in Figs. 3(a) and 3(b), as the width of the Gaussian distribution increases, the illumination tends to become more uniform. Conversely, as the width of the

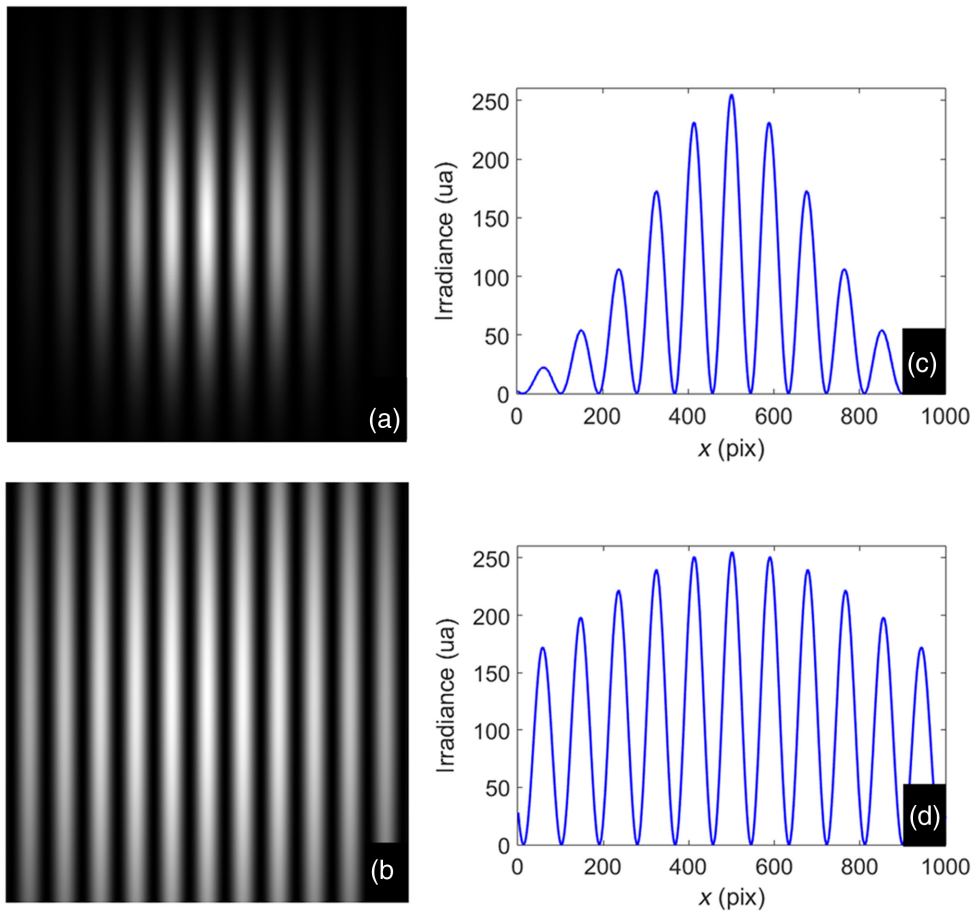


Fig. 3 Varying the background illumination. Interferograms with (a) $\sigma = 0.4$ and (b) $\sigma = 1$, and central profile of images with (c) $\sigma = 0.4$ and (d) $\sigma = 1$.

Gaussian decreases, the image tends to become more illuminated at the center, producing an image with no illumination at the edges. Figures 3(c) and 3(d) are the central profiles of these interferograms, where it can be seen how the inhomogeneous background illumination affects each image.

3 Correlation Coefficient

The correlation coefficient is a measure that indicates the grade of relation that exists between two variables. This relation must somehow be mathematically quantified to show the degree of resemblance. Two images are said to be similar or statistically correlated if they have similar pixel intensities in the same areas.³⁵ If all the values of the variables satisfy an equation exactly, we can say that the variables are perfectly correlated or that there is a perfect correlation between them.

The quantity C , called the correlation coefficient, is given by

$$C = \frac{\sum_{i=1}^n (X_i - \bar{X})(Y_i - \bar{Y})}{\sqrt{\left[\sum_{i=1}^n (X_i - \bar{X})^2 \right] \left[\sum_{i=1}^n (Y_i - \bar{Y})^2 \right]}}, \quad (10)$$

where X and Y are the matrix with the intensity values of the synthetic and experimental interferograms, respectively, while \bar{X} and \bar{Y} are the average of the intensity levels of each interferogram.^{36,37} It must be emphasized that, in every case, the computed value of C measures the degree of the relationship relative to the type of equation that is assumed. Thus, if a linear equation is assumed and Eq. (10) yields a value of C near to zero, in our case, it means that the images that are being compared are not equal, and a value of 1 means that the images are equal.

4 Analysis of the Correlation Behavior

In this section, a detailed analysis of the correlation behavior is shown, when interferograms with different values of visibility, Gaussian noise, and background illumination are evaluated/correlated. Each parameter was analyzed in multiple ways: independently and in combinations of two or three parameters. The correlation value was calculated correlating a perfect synthetic interferogram and a perturbed interferogram.

4.1 Varying the Visibility

To evaluate how the correlation is affected when the visibility is varied in an interference pattern, a set of different interferograms was simulated. For this, in every interferogram, the visibility varied from 0.02 to 1 in increments of 0.02. In Fig. 4, the graph of this analysis is shown.

As can be seen in Fig. 4, the correlation behavior is not affected much by the parameter of visibility, as for values as small as $v = 0.1$, the correlation gives a value of 0.9995, which indicates that we can obtain experimental images with low visibility and the analysis of correlation will not be so affected. Therefore, we can say that the correlation value is almost insensitive to the visibility of the analyzed interferogram.

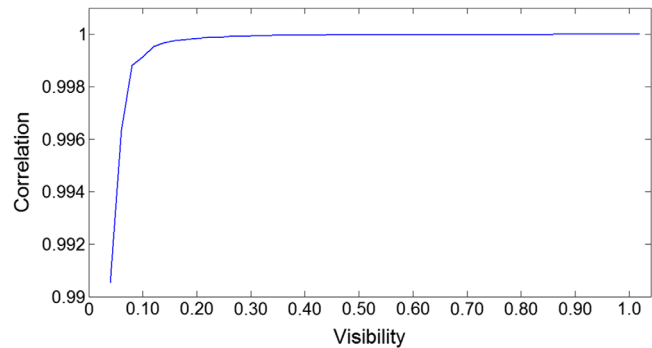


Fig. 4 Correlation behavior when varying the visibility.

4.2 Adding Gaussian Noise to the Interferograms

To understand the correlation behavior when images are affected only by Gaussian noise, interferograms with values ranging from 6.575 to 64.1584 dB were simulated, which corresponds to values of η between 0 and 250. In Fig. 5, a plot can be seen that shows the correlation behavior when these values of Gaussian noise are added to the images.

As can be seen in Fig. 5, the Gaussian noise greatly affects the correlation value, causing it to decrease until it reaches 0.3529 with a PSNR of 6.97 dB, which is rare to obtain because as was mentioned before, when an image is captured at the laboratory, the PSNR values are usually between 20 and 40 dB; in these cases, the correlation value is 0.9735 for 20 dB and 0.9956 for 40 dB.

4.3 Varying the Background Illumination

The last parameter analyzed independently was the background illumination. As was mentioned previously, to simulate synthetic interferograms with inhomogeneous background illumination, it was considered only to add a Gaussian function to the intensity function of the interference patterns (Sec. 2.3). In Fig. 6, the plot of the correlation for every value of sigma, Eq. (8), is shown. For this analysis, sigma increased in every interference pattern, from 0.1 to 5.0 with increments of 0.1.

As can be seen in Fig. 6, the value of correlation falls quickly to 0.1046 for small values of sigma, $\sigma = 0.1$. As the Gaussian width increases, the background illumination of the interference pattern starts to homogenize, and as a result, high values of correlation can be reached. Conversely, when the width of the Gaussian is small, the background illumination is concentrated in the center of the image and the

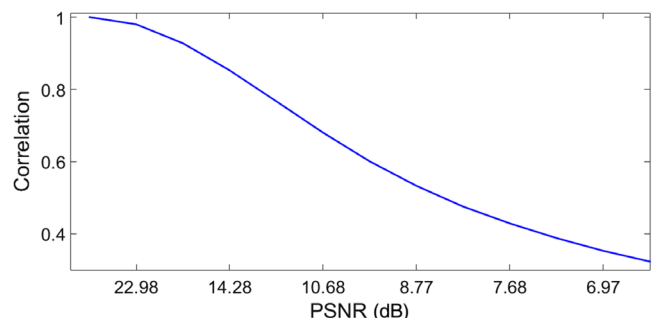


Fig. 5 Correlation behavior when adding Gaussian noise.

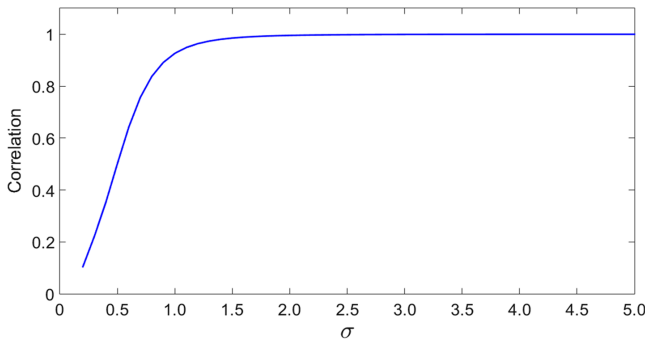


Fig. 6 Correlation behavior when varying the background illumination.

interference pattern is not homogeneous, causing the value of correlation to decrease.

The following sections show the results of the correlation behavior when combinations of these three parameters (visibility, Gaussian noise, and background illumination) degrade the interference patterns.

4.4 Combining Visibility and Background Illumination

The most common factors that affect experimental interferograms in the lab are the visibility combined with inhomogeneous background illumination. In Fig. 7, a plot with the correlation behavior for the combination of these two parameters is shown.

Note in Fig. 7 that, when low visibility and inhomogeneous background illumination are combined in one interferogram, the correlation falls to 0.0185 for a visibility of 0.1 and $\sigma = 0.1$. As mentioned before (Sec. 2.3) for the background illumination, only the width of sigma was varied, not the position of the same, so that, for small values of sigma, the illumination is concentrated at the center of the interference pattern, producing a low illumination at the edges of the image. In addition to the low visibility, the combination of these parameters produces an image almost dark or without information.

For average visibilities that can be obtained in the laboratory, such as $v = 0.5$ and $v = 0.7$, the values of correlation are very similar, so that there will be no difference between a visibility of 0.5 or 0.7 for analyzing an image. Conversely, as the visibility and sigma in the interferogram increase, so will the values of correlation, with a value of 0.9998 for a visibility of 1 and σ greater than 3.5.

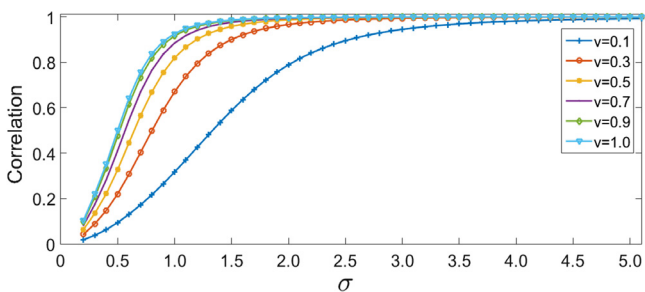


Fig. 7 Correlation behavior combining visibility and background illumination.

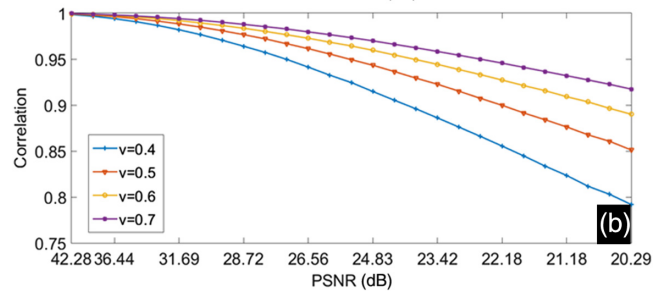
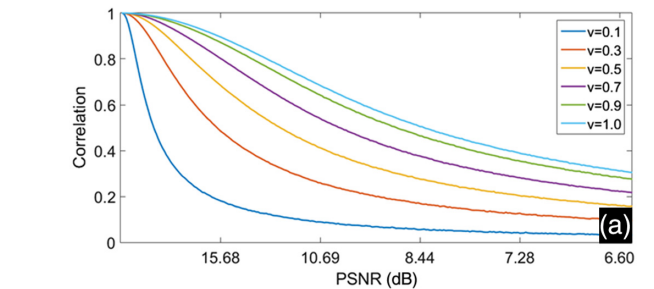


Fig. 8 Correlation behavior combining visibility and Gaussian noise: (a) $6.60 > \text{PSNR} < 20$ and (b) $20.29 > \text{PSNR} < 42.28$.

4.5 Combining Visibility and Gaussian Noise

In Fig. 8(a), a plot of the correlation behavior is shown when changing visibility and Gaussian noise are combined in one interferogram. It can be observed that when Gaussian noise and low values of visibility are combined in one interferogram, the values of correlation are also low. As can be seen, the minimum value of correlation that can be obtained is 0.032 for a visibility of 0.1 and a PSNR of 6.60 dB with $\eta = 250$.

In Fig. 8(b), typical values of visibility (0.4 to 0.7) and PSNR (20 to 40 dB) are shown. The minimum value of correlation was 0.7919 for interferograms with a visibility of 0.4 and $\text{PSNR} = 20.29$.

For images with high values of Gaussian noise and low visibility, the correlation falls to 0.1 for $v = 0.1$ and $\text{PSNR} = 6.60$, although it is rare to have images with high values of Gaussian noise and low visibility.

4.6 Combining Background Illumination and Gaussian Noise

Figure 9 shows the correlation behavior when Gaussian noise and inhomogeneous background illumination are combined in one interference pattern.

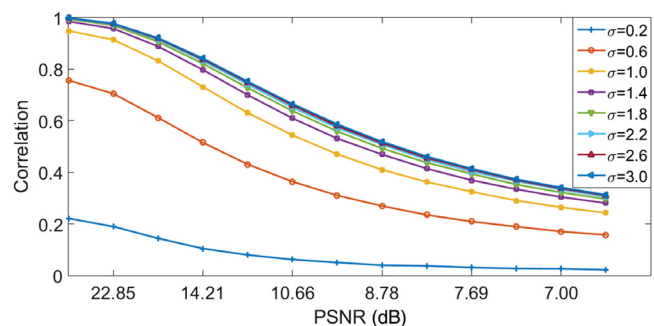


Fig. 9 Correlation behavior combining background illumination and Gaussian noise.

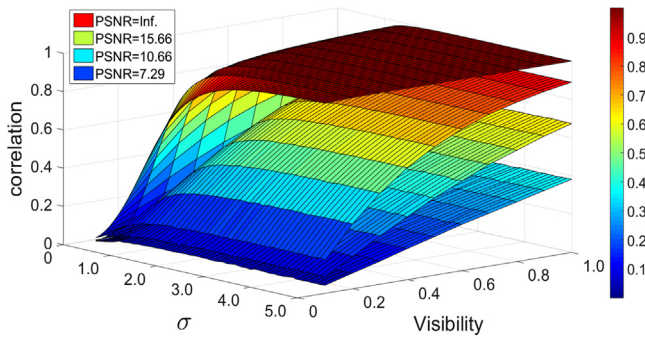


Fig. 10 Correlation behavior combining visibility, background illumination, and Gaussian noise.

Note in Fig. 9 that, for typical values of PSNR, without considering the plot for $\sigma = 0.2$, as it is not common to have an interferogram with this kind of illumination, where only a small zone of the image is illuminated, the combination of Gaussian noise and inhomogeneous background illumination does not greatly affect the correlation, as for a value of $\sigma = 0.6$ and a Gaussian noise of 20 dB, the correlation is 0.7257. This proves again that, as stated in previous sections, the more homogeneous the background illumination in one interferogram is, the greater will be the correlation value. For example, for a background illumination with $\sigma = 3.0$ and a Gaussian noise of $\text{PSNR} \geq 20$, values with a correlation $c > 0.95$ can be obtained.

4.7 Combining Visibility, Background Illumination, and Gaussian Noise

In Fig. 10, the correlation behavior when these three parameters are combined in one interference pattern is shown.

As can be observed in Fig. 10, the combination of visibility, background illumination, and Gaussian noise greatly affects the correlation coefficient. For a visibility of $v = 0.4$, a background illumination of $\sigma = 0.5$, and a Gaussian noise of 10.66 dB, the maximum value of correlation that can be obtained during the analysis of one interferogram is 0.1643. Conversely, when the interference pattern has a good visibility of $v = 0.9$, homogeneous background illumination of $\sigma = 1.5$, and a Gaussian noise of 15.66 dB, the maximum value of correlation that can be obtained is 0.8290. Therefore, it is important to implement an experimental setup, where these three parameters can be avoided or at least be minimal, if high values of correlation are to be reached.

5 Experimental Results

In this section, the analysis of Ronchigrams captured experimentally at the National Institute of Astrophysics, Optics, and Electronics (INAOE)'s instrumentation laboratory is shown. It should be noted that as explained by wave theory, the fringes in the Ronchigram are caused by interference between the overlapping of diffracted wavefronts.^{8,13,19} Therefore, this test can be seen as a lateral displacement interferometer that measures the slopes of the wavefront.

For this analysis, we used the software ReRRCA, described by Aguirre-Aguirre et al.^{19,38} This algorithm was proposed to obtain the wavefront aberrations of ronchigrams, using only one Ronchigram without the need for polynomial fits or trapezoidal integrations. For recovery of the coefficients ν , PSNR, and σ , we followed the process shown in the flowchart of Fig. 11.

Our algorithm has two cycles: the first cycle searches the parameters ν , PSNR, and σ in a wide interval given by the user. The second cycle searches the solution in the form

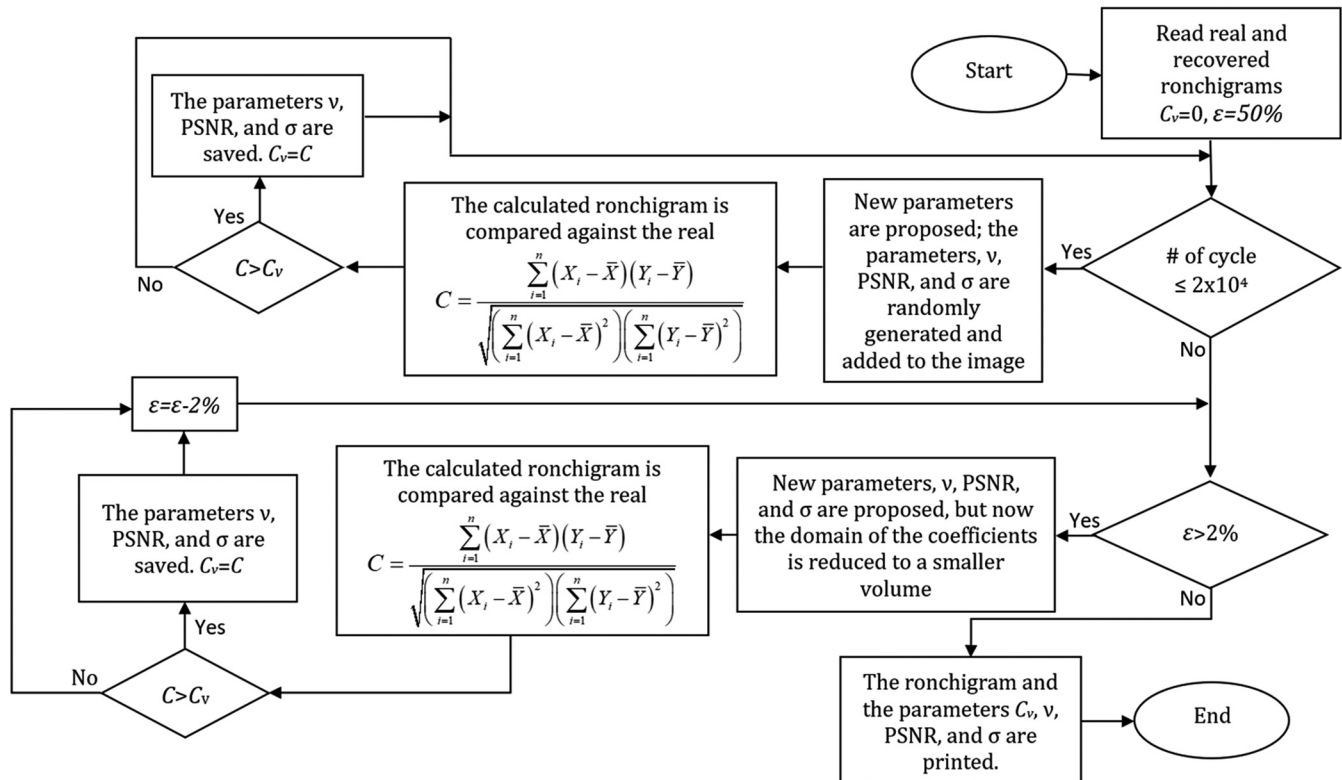


Fig. 11 Flowchart of the proposed algorithm.

Table 1 Design parameters of the surfaces under test.

	Φ (cm)	Radius of curvature (cm)	Conic constant
Surface 1	6.00	59.755	0.00
Surface 2	7.32	53.300	-3.65

$V \pm \varepsilon$, where V corresponds to each parameter ν , PSNR, and σ , and ε takes values from 50% to 2% in steps of 2% of the value of each parameter recovered in the first cycle, these values can change depending on the required accuracy.

For the experimental part, two mirrors were used. In Table 1, their characteristics are shown.

5.1 Spherical Surface

The spherical surface was analyzed using a Ronchi grating of 60 lpi, placed at an intrafocal distance of 1.20 cm. In Fig. 12(a), the experimental image is shown, and in Fig. 12(b), the synthetic Ronchigram calculated by ReRRCA is shown. The correlation between the Ronchigrams was 0.9574.

After the spherical surface was analyzed, the ReRRCA program was modified to calculate the best parameters of visibility, Gaussian noise, and background illumination for the experimental image. For the case of the spherical surface, these values were $\nu = 0.6153$, PSNR = 26.75, and $\sigma = 2.0$.

With these parameters and according to the graph of Fig. 10, the maximum correlation that can be reached is 0.9836, obtaining a difference of 2.66% between the correlation obtained with the experimental image and the correlation that can be reached according to the graph of Fig. 10. The parameters of ν , PSNR, and σ recovered by ReRRCA were used to generate a new image, Fig. 13(a). This synthetic image was correlated with the experimental image of Fig. 12(a), and a correlation of 0.9752 was obtained, with a difference of 2.48% between the correlation of the image with the parameter fitted and the maximum correlation that can be reached ($C = 1$).

In Fig. 13(b), the plots of the central irradiance profiles of the images of Figs. 12(a) and 13(a) are shown. Note that the profiles of the two images are very similar, both in visibility and in background illumination.

5.2 Hyperbolic Surface

A hyperbolic surface was analyzed with a Ronchi grating of 80 lpp, placed at an intrafocal distance of 0.430 cm from the center of curvature. In Fig. 14(a), the experimental image is shown, and in Fig. 14(b), the Ronchigram recovered with ReRRCA is shown. The correlation between the Ronchigrams was 0.5943.

The results obtained by ReRRCA for the values of ν , PSNR, and σ were 0.4830, 31.93, and 0.7150, respectively. As is shown in the plot of Fig. 10, the maximum correlation that can be reached is 0.6689, with a difference of 11.15%

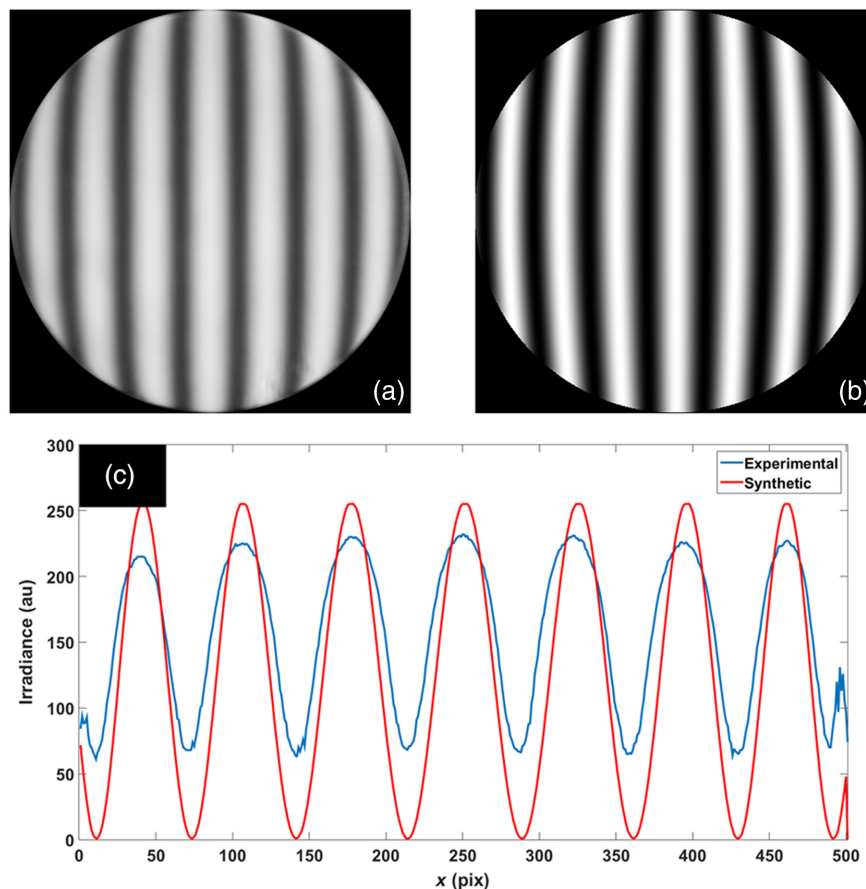


Fig. 12 Spherical surface: (a) experimental, (b) synthetic Ronchigrams, and (c) central profiles of (a) and (b).

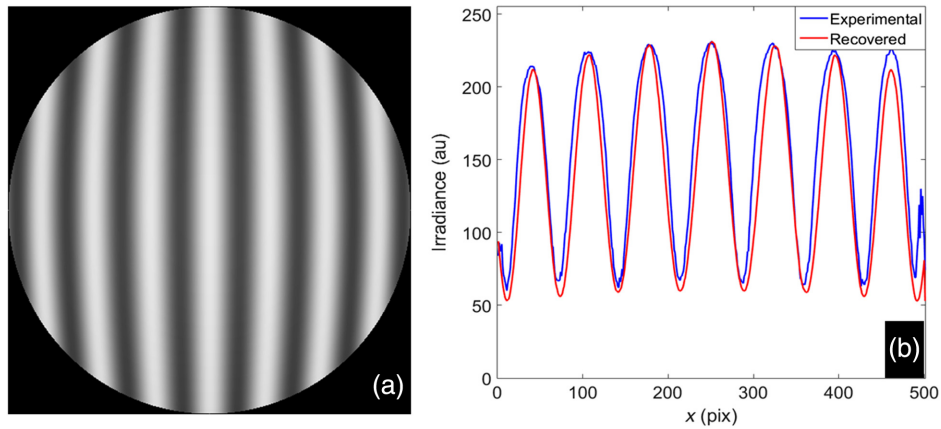


Fig. 13 (a) Synthetic Ronchigram of the spherical surface adding the values recovered with ReRRCA, $\nu = 0.6153$, PSNR = 26.75, and $\sigma = 2.0$, and (b) central profiles of Figs. 11(a) and 12(a).

between the correlation obtained with the experimental image and the correlation that can be reached according to the graph of Fig. 10.

The experimental image of Fig. 14(a) was correlated with the synthetic Ronchigram generated with the parameters of ν , PSNR, and σ recovered by ReRRCA [Fig. 15(a)]. The correlation was 0.8940, with a difference of 10.60% between the correlation of the synthetic image with the parameters fitted and the maximum correlation that can be reached ($C = 1$). In Fig. 15(b), a central profile of the images of Figs. 14(a)

and 15(a) is shown, where it can be seen that the profile of the two images does not match in a good manner, which means that the surface that is being fabricated is far from the ideal surface that is intended to be obtained.

With this analysis, the influence that the visibility, the Gaussian noise, and the inhomogeneous background illumination have over the correlation can be seen. Therefore, it is recommended to capture images avoiding inhomogeneous background illumination, low visibility, and Gaussian noise. Another recommendation or alternative could be to have

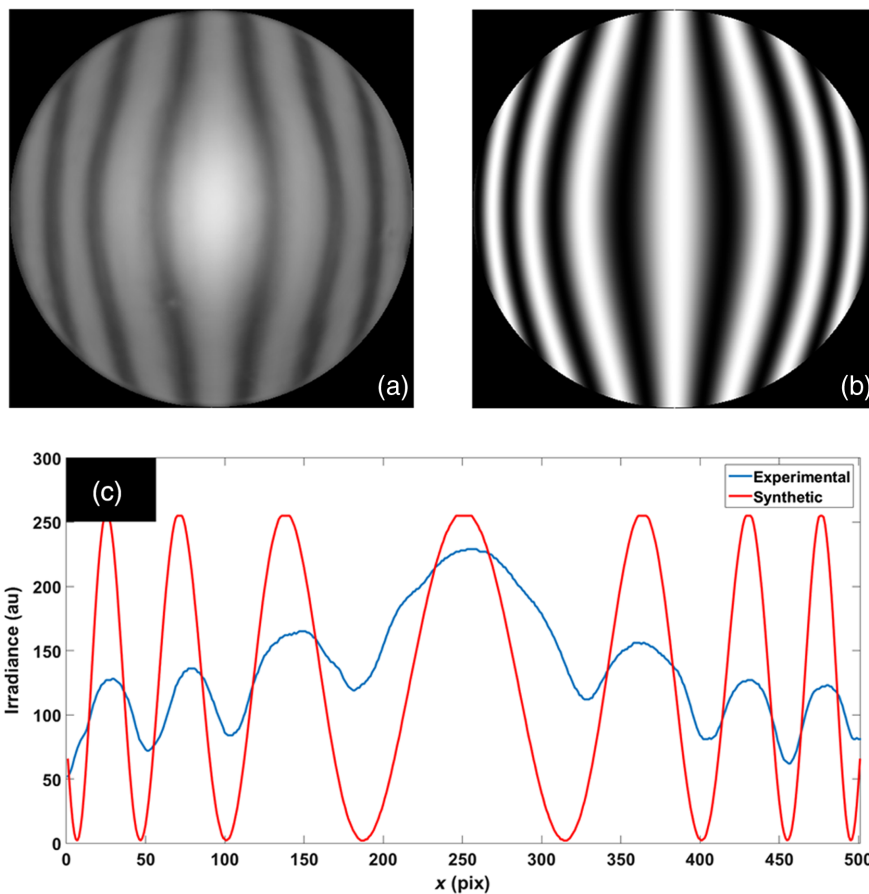


Fig. 14 Hyperbolic surface: (a) experimental, (b) synthetic Ronchigrams, and (c) central profiles of (a) and (b).

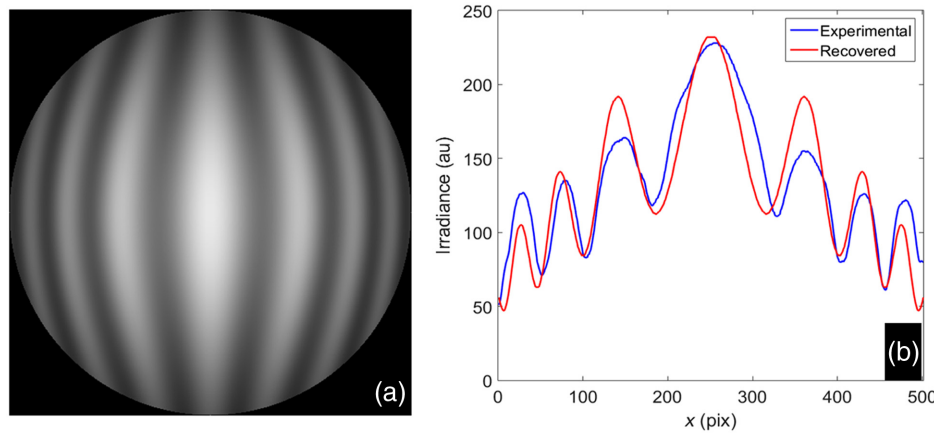


Fig. 15 (a) Synthetic Ronchigram of the hyperbolic surface adding the values recovered with ReRRCA, $\nu = 0.4830$, PSNR = 31.93, and $\sigma = 0.7150$, and (b) central profiles of Figs. 14(a) and 15(a).

some method for calculating ν , PSNR, and σ from the experimental image, so that these values can be added to the synthetic interferogram or subtracted from the experimental one. By undergoing this process, a correlation value of 1 could be reached, and a criterion for knowing when an optical surface is finished could be implemented.

6 Conclusions

A study to analyze the correlation behavior during the evaluation of interferograms with different values of visibility, Gaussian noise, and background illumination was presented in this work. It was proved that, when an interferogram is affected by these parameters, the factor that most affects the correlation is an inhomogeneous background illumination, as for low values of sigma, the correlation falls to 0.1046 for $\sigma = 0.1$. This is not the case for low visibilities, where the maximum value of correlation that can be reached is 0.9995 with a visibility of $\nu = 0.1$. Conversely, when an interference pattern is deteriorated by Gaussian noise, the minimum value of correlation that can be reached is 0.3529 with a PSNR of 6.97 dB, although it is uncommon to capture an interferogram with this noise level.

The combination that most affects the correlation is the combination of visibility with inhomogeneous background illumination, where the minimum correlation value was 0.0185 with a visibility of 0.1 and $\sigma = 0.1$. For the combination of background illumination with Gaussian noise, the minimum value of correlation reached was 0.1575 for $\sigma = 0.6$ and Gaussian noise of 6.97 dB.

The least disruptive combination for the correlation analysis was for the case of visibility combined with Gaussian noise, where for a value of $\nu = 0.4$ and a PSNR of 20.29 dB, the minimum value of correlation reached was 0.7919.

It was proved that the combination of visibility, Gaussian noise, and inhomogeneous background illumination greatly affects the value of the correlation, where for a visibility of $\nu = 0.4$, $\sigma = 1.5$, and a PSNR of 15.66 dB, the maximum value of correlation reached during the analysis of one interferogram was 0.5289.

Finally, the correlation coefficient was used to analyze real surfaces. It was demonstrated that when the parameters of visibility, background illumination, and Gaussian noise can be calculated from the experimental image, it will ensure

that a correlation value very close to 1 can be reached, and a criterion for knowing when an optical surface is finished can be implemented.

Acknowledgments

We are grateful for the financial support for this project from the Dirección General de Asuntos del Personal Académico (DGAPA)-UNAM, through the grant PAPIIT No: TA100217 "Sistema de medición de objetos reflectores utilizados en la industria automotriz basado en la prueba de pantallas nulas y algoritmos probabilistas." B.V.-M. would thank the CONACyT for the postdoctoral scholarship granted.

References

1. J. B. Saunders, "A simple interferometric method for workshop testing of optics," *Appl. Opt.* **9**(7), 1623–1629 (1970).
2. B. E. Truax, "Absolute interferometric testing of spherical surfaces," *Proc. SPIE* **1400**, 61–68 (1991).
3. D. G. Kocher, "Twyman-Green interferometer to test large aperture optical systems," *Appl. Opt.* **11**(8), 1872–1874 (1972).
4. D. Malacara and A. Cornejo, "Testing of aspherical surfaces with Newton fringes," *Appl. Opt.* **9**(4), 837–839 (1970).
5. J. S. M. Núñez et al., "Interferómetro de Fizeau Para Prueba de Superficies Ópticas," *Internal Report*, IA-UNAM (2004).
6. J. H. Burge, "Fizeau interferometry for large convex surfaces," *Proc. SPIE* **2536**, 127–138 (1995).
7. J. Schwider and O. R. Falkenstoerfer, "Twyman-Green interferometer for testing microspheres," *Opt. Eng.* **34**(10), 2972–2975 (1995).
8. D. Malacara, Z. Malacara, and M. Servin, *Interferogram Analysis for Optical Testing*, 2nd ed., Taylor & Francis, New York (2005).
9. K. Creath and J. C. Wyant, "Direct phase measurement of aspheric surface contours," *Proc. SPIE* **0645**, 101–106 (1986).
10. K. Hibino et al., "Tunable phase-extraction formulae for simultaneous shape measurement of multiple surfaces with wavelength-shifting interferometry," *Opt. Express* **12**(23), 5579–5594 (2004).
11. G. H. Kaufmann and G. E. Galizzi, "Evaluation of a method to determine interferometric phase derivatives," *Opt. Laser Eng.* **27**(5), 451–465 (1997).
12. E. Robin and V. Valle, "Phase demodulation from a single fringe pattern based on a correlation technique," *Appl. Opt.* **43**(22), 4355–4361 (2004).
13. D. Malacara, *Optical Shop Testing*, 3rd ed., John Wiley & Sons, Hoboken, New Jersey (2006).
14. J. Millerd et al., "Modern approaches in phase measuring metrology," *Proc. SPIE* **5856**, 14–22 (2005).
15. J. P. Hot and C. Durou, "System for the automatic analysis of interferograms obtained by holographic interferometry," *Proc. SPIE* **0210**, 144–153 (1980).
16. D. A. Tichenor and V. P. Madsen, "Computer analysis of holographic interferograms for nondestructive testing," *Opt. Eng.* **18**(5), 469–472 (1979).
17. J. C. Hunter, M. W. Collins, and B. A. Tozer, "An assessment of some image enhancement routines For use with an automatic fringe tracking programme," *Proc. SPIE* **1163**, 83–94 (1989).

18. D. H. Penalver, D. L. Romero-Antequera, and F. S. Granados-Agustín, "Interferogram smoothing and skeletonizing using Bessel functions of the first kind," *Opt. Eng.* **51**(4), 045601 (2012).
19. D. Aguirre-Aguirre et al., "Algorithm for Ronchigram recovery with random aberrations coefficients," *Opt. Eng.* **52**(5), 053606 (2013).
20. B. Villalobos-Mendoza et al., "Phase shifting interferometry using a spatial light modulator to measure optical thin films," *Appl. Opt.* **54**(26), 7997–8003 (2015).
21. X. Su and W. Chen, "Fourier transform profilometry: a review," *Opt. Lasers Eng.* **35**(5), 263–284 (2001).
22. K. H. Womack, "Interferometric phase measurement using spatial synchronous detection," *Opt. Eng.* **23**(4), 234391 (1984).
23. J. J. Sánchez-Escobar, J. H. Pascual Alonso-Magaña, and S. Vázquez-Montiel, "Obtaining the wavefront aberrations of a real interferogram by use of a hybrid genetic algorithm," *Opt. Eng.* **45**(10), 105605 (2006).
24. A. Cordero-Dávila and J. González-García, "Optical surface evaluation by correlating bi-Ronchigram images," *Opt. Eng.* **54**(3), 034108 (2015).
25. S. Vázquez-Montiel, J. J. Sánchez-Escobar, and O. Fuentes, "Obtaining the phase of an interferogram by use of an evolution strategy: Part I," *Appl. Opt.* **41**(17), 3448–3452 (2002).
26. S. Vázquez-Montiel and J. J. Sánchez-Escobar, "Experimental interferogram analysis using an automatic polynomial fitting method based on evolutionary computation," *Opt. Eng.* **44**(4), 045604 (2005).
27. M. Born, *Principles of Optics*, 4th ed., Pergamon Press, New York (1980).
28. E. Hecht, *Optics*, 4th ed., Addison-Wesley, San Francisco (2002).
29. T. Kreis, *Handbook of Holographic Interferometry: Optical and Digital Methods*, Wiley-VCH, Weinheim (2005).
30. Y. Surrel, "Additive noise effect in digital phase detection," *Appl. Opt.* **36**(1), 271 (1997).
31. T. Yoshizawa, *Handbook of Optical Metrology: Principles and Applications*, 2nd ed., CRC Press, Yokohama (2015).
32. D. Báez López and O. Cervantes Villagómez, *MATLAB Con Aplicaciones a La Ingeniería, Física Y Finanzas*, 2nd ed., Alfaomega, México (2012).
33. D. Salomon and G. Motta, *Handbook of Data Compression*, 5th ed., Springer, Northridge (2010).
34. D. Aguirre-Aguirre, "Prueba Nula de Ronchi Dinámica," PhD Thesis, INAOE (2014).
35. S. Ait-Aoudia, F. Z. Benhamida, and M. A. Yousfi, "Lossless compression of volumetric medical data," *Lect. Notes Comput. Sci.* **4263**, 563–571 (2006).
36. M. R. Spiegel, J. J. Schiller, and R. A. Srinivasan, *Probability and Statistics*, 4th ed., Mc Graw Hill, New York (2013).
37. M. R. Spiegel and L. J. Stephens, *Schaum's Outline of Theory and Problems of Statistics*, 3rd ed., McGraw-Hill, New York (1999).
38. D. Aguirre-Aguirre et al., "Fast conical surfaces evaluation with null-screens and randomized algorithms," *Appl. Opt.* **56**(5), 1370–1382 (2017).

Brenda Villalobos-Mendoza is a member of SPIE, currently, she is a postdoctoral researcher at Centro de Investigación y de Estudios Avanzados del Instituto Politécnico Nacional in Monterrey, Mexico. She received her engineering degree from the UACJ, Mexico, in 2008, her MS degree in optics from Benemérita Universidad Autónoma de Puebla (BUAP), Puebla, Mexico, in 2010, and her PhD degree in optics from the Instituto Nacional de Astrofísica Óptica y Electrónica (INAOE), Puebla, Mexico, in 2015. She has experience in optical testing in the laboratory and her research interests includes interferometric optical testing and phase-shifting interferometry.

Daniel Aguirre-Aguirre is a researcher in the Department of Optics and Microwaves in the Institute of Applied Sciences and Technology at the UNAM, Mexico. He received his engineering physics degree in 2007 from the Institute of Engineering and Technology at the UACJ, Mexico. He received his MS and PhD degrees in optics in 2010 and 2014, respectively, both from the National Institute of Astrophysics, Optics, and Electronics (INAOE), Puebla, Mexico. His current research interests include optical metrology, digital image processing, and optical instrumentation. He is a member of SPIE.

Fermín Granados-Agustín is a researcher in the Optics Department of the National Institute of Astrophysics, Optics, and Electronics INAOE, Mexico. He received his BS degree in physics from the National University of Mexico UNAM, in 1993. He received his MS and PhD degrees in optics, respectively, in 1995 and 1998, both from the INAOE. He is a national researcher for the National System of Researchers, Mexico. He held a postdoctoral position at the Mirror Lab of the Steward Observatory at the University of Arizona, in 1999. His research interests included optical information, interferometric optical testing, and instrumentation.